

A failure incident occurred on perforated casing tubing for geothermal wells. The damage happened during the drilling process by an air drilling technique after eleven days from the installation. Even though air drilling is a common method for geothermal drilling, this incident showed a lesson to learn to prevent a similar accident in the future. Failure analysis based on the laboratory and field observation was done to get the failure incident's root cause. The visual identification result showed a severe depletion and cracks in the tubing at a depth of 1,450–1,500 m. Optical emission spectroscopy and the tensile test showed materials appropriateness to the specifications. The corrosion attacked from the outer side of the tube. This tubing was exposed to an environment with significant H₂S, CO₂, water steam, and oxygen from the air drilling process. The results of X-ray diffraction analysis (XRD) showed FeS and Fe₃O₄ in the corrosion product. Both of the scale formed as a different layer, where the FeS is formed below the Fe₃O₄ layer. The energy dispersive spectroscopy (EDS) results revealed that each tubing's sulfur content gets an increase in the deeper location. The gas sampling result showed that H₂S gas is more dominant than CO₂ gas, which showed the sour service condition. Corrosion rate calculation modeling was also performed based on the environment parameter; the result is lower than the real cases. The oxygen from air drilling also accelerates the corrosion rate as it acted as an oxidizing agent in the process. Free sulfur is possibly formed, which is possibly transformed into sulfuric acid. This study showed the lesson learn about the deadly combination of sulfur, oxygen, H₂S, and CO₂, making a severe corrosion rate in the perforated tubing

Keywords: corrosion, H₂S, air drilling, failure, tubing, failure analysis, carbon steel

Received date 23.10.2020

Accepted date 07.12.2020

Published date 22.12.2020

Copyright © 2020, Harris Prabowo, Yudha Pratesa, Askin Tohari,

Ali Mudakir, Badrul Munir, Johnny W. Soedarsono

This is an open access article under the CC BY license (<http://creativecommons.org/licenses/by/4.0>)

1. Introduction

Geothermal energy is one of the promising renewable energy in the future. However, the drilling process for a geothermal field has many challenges due to its complex characteristics. The most common problems are corrosion, fatigue, thermal, and erosion [1].

Geothermal drilling is a complicated process. The drilling process material will be faced with extreme environments, namely high-temperature environments, and highly corrosive gases such as H₂S, CO₂, and water vapor. In addition to corrosive environments, the hard rock released during the drilling makes possible erosion-corrosion [2, 3].

Air drilling is a pneumatic percussion drilling using gases, usually compressed air or nitrogen, to cool the drill bit and lift the wellbore residual compared to conventional drilling using liquids. It is an inexpensive and effective drilling method [4].

The air drilling could accidentally bring some oxygen into the environment, producing elemental sulfur after reacting with some H₂S from the reservoir [5]. The corrosion rate increased significantly due to the corrosion product's porous structure under a mixture of H₂S and O₂ gas environment. Yong Hua et al. found SO₂ and O₂ to make seven times higher compared without SO₂ environment due to the change of Fe₂CO₃ to FeSO₃.H₂O [6]. The effect of oxygen in the mixture of the SO₂-CO₂ system is also found in the

UDC 620.193

DOI: 10.15587/1729-4061.2020.215163

FAILURE ANALYSIS OF GEOTHERMAL PERFORATED CASING TUBING IN H₂S AND O₂ CONTAINING ENVIRONMENT

Harris Prabowo

Master of Science, Doctorate Candidate*

E-mail : h_prabowo@pertamina.com

Yudha Pratesa

Master of Engineering*

E-mail: yudha@metal.ui.ac.id

Askin Tohari

Master of Science

PT Pertamina Geothermal Energy

Jl. Medan Merdeka Timur, 1A, Jakarta, Indonesia, 1011

E-mail: askinth@pertamina.com

Ali Mudakir

Master of Science

PT Elnusa

Jl. TB Simatupang Kav. 1 B, Graha Elnusa, Jakarta, Indonesia, 12560

E-mail: Amundakir@pertamina.com

Badrul Munir

Associate Professor*

E-mail: bmunir@ui.ac.id

Johnny W. Soedarsono

Professor*

E-mail : jwsono@metal.ui.ac.id.

*Department of Metallurgy and Materials

Universitas Indonesia

Kampus Baru UI-Depok, Indonesia

corrosion rate of Cr-steel material even though with a lower magnitude [7].

Therefore, studies are devoted to finding the root cause of tube failure, which could contain a mixture of complex gas such as $\text{CO}_2\text{-H}_2\text{S-O}_2$. This study will give a lesson to learn about the possible effect of O_2 in the geothermal system that contains a significant amount of H_2S .

2. Literature review and problem statement

The geothermal reservoir contains several non-compressed gases such as H_2S , CO_2 , and methane. Those gases are known to be a corrosive agent when diffused into the reservoir water. If the environment is saturated with CO_2 gas, a sweet corrosion mechanism happens [8]. Sour corrosion is another possibility of failure in geothermal tubing. Sour corrosion usually happens in H_2S -rich reservoirs where the partial pressure of $P_p \text{CO}_2/P_p \text{H}_2\text{S}$ is less than 20 [9].

In a sour corrosion environment, the attack evidence is manifested by crack if carbon steel has a hardness of more than 23 HRC [10]. Blisters are formed due to hydrogen diffusion into the metal lattice and create stresses in the material lattice [11]. The corrosion product from sour corrosion was FeS [12]. However, H_2S corrosion could become severe under the influence of oxygen or SO_2 polluted environment [6, 13]. Oxygen reduces the possibilities of hydrogen diffusion into the iron lattice, hence prevents crack formation [13]. Song et al. found oxidized sulfur specie sulfate (SO_4^{2-}) at all temperatures, whereas liquid still exists [14]. Another study by Sun et al. showed similar results with Song et al. The sulfate ion exists in the $\text{H}_2\text{S-O}_2$ system and lowers the pH solution. This system resulted in a severe corrosion rate even for chromium-containing steel [7].

However, most of the results happen below 100°C and under the laboratory examination. Our study will show the real example of the effect of oxygen, SO_2 , and CO_2 in the high-temperature environment, in this case a geothermal system.

3. The aim and objectives of the study

The aim of the study is to learn about the possibility of tubing failure due to a combination of CO_2 , H_2S , and O_2 environment.

To achieve this aim, the following objectives are accomplished:

- elaboration of field observation and visual data of the tube to get the environmental parameter and effect on the tubing;
- materials characterization using metallography, optical emission spectroscopy, and tensile test to check materials specification;
- conducting a CO_2 corrosion modeling calculation using the NORSOK standard to get an estimation value of corrosion rate;
- conducting scanning electron microscopy, energy dispersive spectroscopy, and XRD for scale analysis that formed in the tube.

4. Materials and methods of research

A failure analysis method was conducted based on the laboratory examination and field observation to achieve the

objectives. Many failure possibilities were checked carefully, such as material defects, environmental effects, or anomalies operations. The specimens were taken from several depths of the tube and were cut with a water-cooled band saw. The macrographics observations were performed using the Olympus stereomicroscope. The surface preparation was started from 120 to 2,500 mesh using SiC paper before polishing with step with alumina powder. Microstructural observations were conducted using 2 % nital (2 % nitric acid (HNO_3) and 98 % (ethyl) alcohol $\text{C}_2\text{H}_5\text{OH}$ mixture) as the etching solution after polishing with diamond paste. Each grinding step was rinsed in water to remove the residual SiC powder. The etching process was performed between 10–15 seconds. All of the etching solution is under fresh solution and directly used after the mixing. The specimen was analyzed by the Olympus microscope under 100x magnification to get the banding pattern of microstructure as an indication of rolled products.

Chemical composition samples were taken from the upper section and lower section of the drilling tube, then tested with optical emission spectroscopy using WAS spectrometry. The specimen was ground to get a fresh surface until 300 mesh with SiC paper.

Mechanical properties were represented with hardness and tensile tests. The position of each test specimen is shown in Fig. 1. Tensile testing was conducted by 20 tons Shimadzu universal testing machine and tensile test specimens were prepared based on ASTM E8. Hardness test was performed using a Rockwell B hardness test based on ASTM E18 with at least five indentations made for each sample for the average value. Cutting and preparation were performed under the water-cooled cutting process to prevent overheating.

FEI Inspect 50 field emission scanning electron microscope (Fe-SEM) was used for an in-depth study of scale morphology on the corroded perforated tube, and energy dispersive spectroscopy (EDS) equipped the chemical composition of each scale layer with backscattered mode. The scale was taken from the internal side of the tube and stored under a special plastic container to prevent any composition change.

X-ray diffractometer (XRD) examination was performed using a Phillips X-ray diffractometer (XRD) with $\text{K}\alpha$ Cu as the electron source using a scan rate of $2^\circ/\text{min}$. The result was analyzed with MATCH! With Rietveld refinement.

4. 1. Field observation

The tubing fracture was found at casing #57–62 with the vertical depth of 1,450–1,500 m below the sea level. This area is the total loss area, where the steam is found. The tubing was severely corroded with the remaining thickness around 1–3 mm, only several days. The tubing was covered by a yellowish scale, especially at casing #60–62.

The perforated hole morphology widened parallel to the flow direction. Based on the gas analysis, the well has 0.2 % wt non-compressed gas (NCG), which consists of 53 % mole CO_2 and 9 % mole H_2S . The schematic position of the failed tube is shown in Fig. 1.

It had a sour service operation with pH 4.51. The pressure of the well was 155 psig. The partial pressure of CO_2 was 106 psig, while H_2S was 10.2 psig. It also contains oxygen from the air drilling; however, the amount of oxygen gas cannot be measured during the drilling process. The result of gas sampling is shown in Table 1.

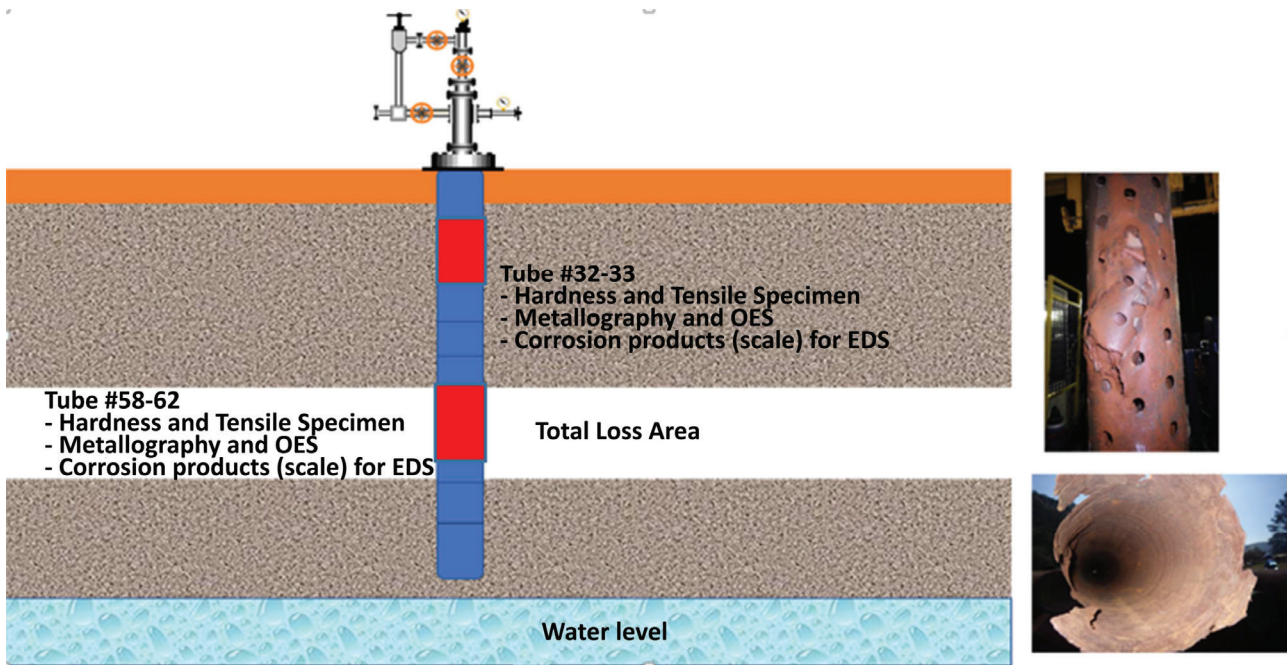


Fig. 1. Position of perforated tubings leak

Table 1

Gas sampling from the well			
CO ₂ (%)	H ₂ S (%)	NH ₃ (%)	Ar (%)
53	9	0.6	0.4

All of the data from the field observation are used in the corrosion rate calculation as shown in section 6.

4. 2. Corrosion rate calculation

NORSOK M506 is used to calculate the rate of corrosion by CO₂ (sweet corrosion) [8]. The corrosion rate is calculated by entering several known parameters from well conditions such as temperature, CO₂ gas content, pressure, amount of water, and gas produced. Several other parameters were omitted because there were no supporting data, such as glycol and corrosion inhibitors.

The corrosion rate was modeled by eq. (1). This equation is suitable for the corrosion rate of 120 °C.

$$CRt \text{ (mm/yr)} = Kt \times f_{CO} \times 20.62 \times (S/19) \times \times 0.146 + 0.0324 \log(f_{CO_2}) \times f(\text{pH})t, \tag{1}$$

where *Kt* is a constant based on temperature, which is calculated from a linear extrapolation of corrosion rate at above and below interested temperature, fugacity of CO₂ (*f*_{CO}) and pH at the desired temperature *f*(pH) were measured directly from the fluid and gas sampling. The shear stress was calculated from eq. (2) using the data production, with several assumptions.

$$S \text{ (Pa)} = 0.5 \times \rho_m \times f \times u_m^2, \tag{2}$$

where (*f*) is friction factor, ρ_m is mixture density of gas and water, while *u_m* is kinematic viscosity.

The result showed that the CO₂ corrosion rate is around 10 mm/year. This corrosion rate magnitude is not enough to answer this incident's root cause since this failure happened before one year of operation. So, there should be another ex-

planation for this high corrosion rate. The presence of H₂S or erosion-corrosion should be elaborated further.

5. Result of laboratory analysis of corroded tube

5. 1. Result of visual examination

Visual examination is performed only on the specific tube where the severe corrosion occurred. Casing number 60 was attacked by external and internal corrosion. However, casing number #57–58 is only attacked by external corrosion. Casing number #62 was attacked by external corrosion. However, it has a different corrosion pattern compared to the casing number 57–58 as shown in Fig. 2. At casing above #60, the corrosion leaves a uniform and large crater on the external side of the tubing.

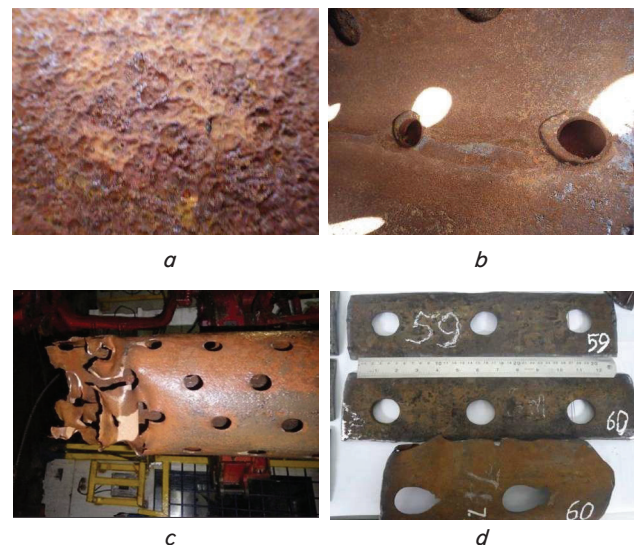


Fig. 2. Visual condition of casing tubing a – external; b – internal side condition of tubing; c – after fishing; d – external condition of each tubing

At the upper-level tubing, the corrosion was smooth, as shown in Fig. 2, *d*. Besides the corrosion morphology, as a higher depth of tubing, the corrosion product color is changing. The lower-level tube will have a more yellowish color, while the upper-level tube will be brownish.

5. 2. Result of materials conformity

The result of material conformity did not show any significant difference between casing tubing #38, 58, 59 and 60 from the chemical composition aspect, as shown in Table 2. The composition of phosphor and sulfur in materials met the materials specification. There is no issue of the fabrication defect. All the casing-tubing test results correspond to the API 5CT grade K55 standard materials.

The hardness test result from the casing is still below the maximum limit for sulfide stress cracking (SSC). It had a hardness number of around 94 HRB (16 HRC). Based on NACE MR 0176, the hardness number of carbon steel should be less than 23 HRC to prevent the SSC. Table 3 showed that both #38 and #59 tubing have a similar number of mechanical properties. It means that the specimen did not suffer severe temperatures that could change the microstructure.

Table 2

OES testing result of each tubing

Material	C (%)	P (%)	S (%)	Fe (%)
#60	0.234	0.011	<0.003	97.4
#38	0.225	0.009	<0.003	97.4
#58	0.225	0.012	<0.003	97.4
#59	0.227	0.012	<0.003	97.3
API 5CT K55	Ns	0.03max	0.030max	Ns

Table 3

Mechanical properties of API 5CT

Sample	Tensile Str (kgf/mm ²)	Yield Str (kgf/mm ²)	El (%)	Hardness (HRB)
#38	73	46	23	94
#59	78	57	23	96
API 5CT	66.79 min	38.7–56	18 min	

There is a little change in yield strength between tubing #38 and #59, but the changes are still fit with the yield strength of API 5CT tubing.

5. 3. Result of scale analysis

A pinch of corrosion products was taken from several positions at the external side of the tubing. EDS analysis is performed in several positions, and the representative result is given in Table 4. The result showed that the scale consists of a significant amount of sulfur, carbon, oxygen, and chloride. Two elements, silicon and sulfur, obviously increase as the depth is increased. A considerable amount of sulfur indicated that the reservoir contains H₂S from gas or S from the rock formation. The highest sulfur content was detected in casing tubing No. 60, which has the most severe corrosion and the location where the failure occurred. The

presence of silicon could be an indication of sand/stone debris from the reservoir.

Table 4

Distribution of each element in corrosion product from top position to the lowest tubing

Element (%)	#58	#59	#60	#62
O	44.8	40.5	32.2	28.7
Al	0.2	0.28	1.8	00.8
Si	0.3	0.2	4.14	1.0
S	8.5	12.0	31.7	53.5
Fe	46.1	46.9	30.1	16.0

Fig. 3 showed the X-ray diffraction (XRD) result of corrosion products. It is found that magnetite and iron sulfide (FeS) dominated in the scale compound. Magnetite was formed by the oxidation process, while iron sulfide was a product of material and hydrogen sulfide reaction. This result indicated that casing tubing 60 exposed to them an abundance of H₂S gas service. Siderite (Fe₂CO₃) was not detected even though the environment had significant amounts of CO₂ gas.

Scanning electron microscopy was conducted at corrosion products. The examination was taken on the inner side of the corrosion product. The result showed the formation of two layers of corrosion products. The first layer is iron sulfide (FeS) covered by magnetite (Fe₃O₄) as the second layer. The result is shown in Fig. 4.

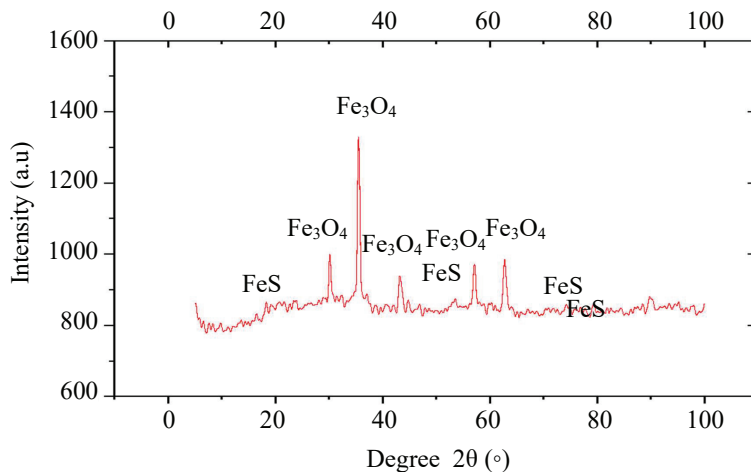


Fig. 3. XRD test result of corrosion product

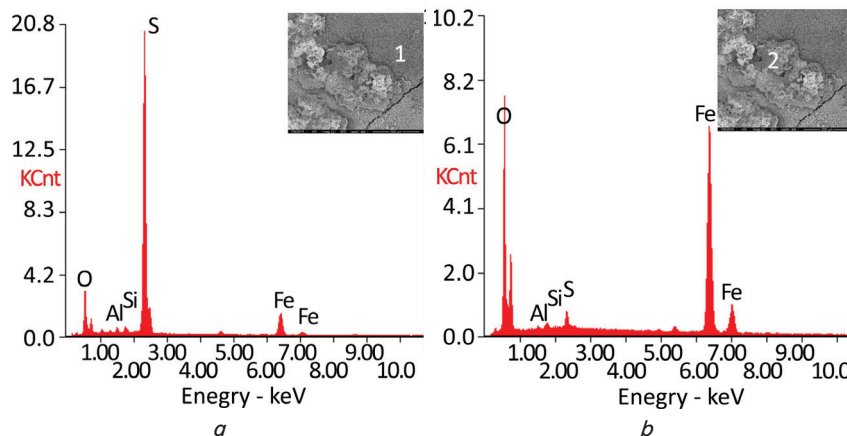


Fig. 4. Corrosion product consisting of different layers: *a* – iron oxide; *b* – iron sulfide

EDS observations showed an increase in sulfur content concomitant with the depth. Sulfur increased significantly after casing No. 60, which is a position where a total loss was found. It could be an indication of a gas pocket found in that area.

5. 4. Result of metallographic examination

Microstructure analysis was done to investigate the effect of temperature or manufacturing defect. Fig. 5 was taken in a cross-section area and compared between tubing No. 38 and 60. The result reveals no differences in microstructure from casing 60 and 38. Both microstructures had pearlite (dark phase) and ferrite (white phase). The pearlite showed a pearlite band, which is a typical result of the extrusion product.

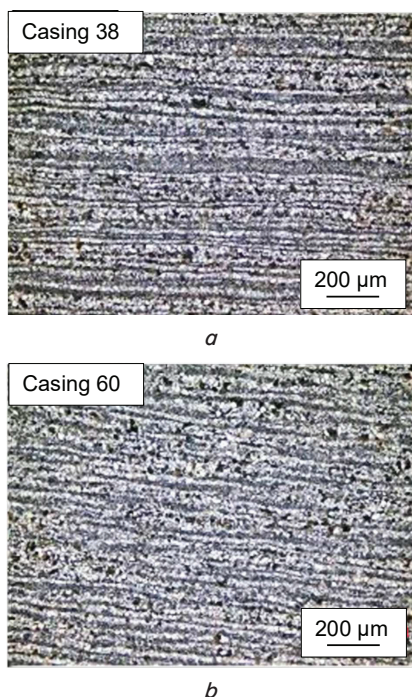


Fig. 5. Metallography of: *a* – normal casing; *b* – failure casing showed similar structure

All of the tubings had similar grain size numbers and did not show any grain growth or creep evidence. It revealed no indication of high-temperature condition exposure. Similar microstructure from both casing tubing indicated the failure did not relate with the material defects. There is no macro porosities nor crack found in both of the tubes.

6. Discussion of research results of failure perforated tube

From the visual and thickness measurement, the rate of corrosion attack is greater at lower tubing depth. Joint No. 60 was the most severe. Casing tubing 60 failed in the middle of the tubing and showed plastic deformation at the fracture area. Plastic deformation is an indication of excessive load that happens at the material. Crack propagated circumferential and longitudinal at the tube 60. This crack could have resulted from the fishing process (circumferential crack) or the effect of thickness depletion (longitudinal crack).

The metallographic, chemical composition (OES), and mechanical test (tensile test) did not indicate material defect contributed to this failure. Casing tubing k-55 grade material is commonly used for the general environment where CO₂ corrosion or H₂S corrosion is not dominant in the reservoir. It is classified as carbon steel casing tubing, which has moderate mechanical properties.

Hardness test of casing tubing materials revealed it did not surpass the maximum hardness for stress sulfide cracking in NACE MR0175 standard. It confirms the crack was caused by the revocation process of the casing from the reservoir and not related to the failure event.

From the visual examination, corrosion is more dominant in causing damage to the casing. Due to the mixture of CO₂ and H₂S gasses in the environment, the partial pressure of H₂S and CO₂ is important to know. Three types of conditions will occur in the CO₂/H₂S environment.

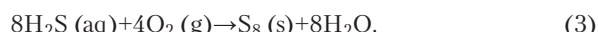
Table 5

Sour and sweet corrosion partial pressure parameters [9]

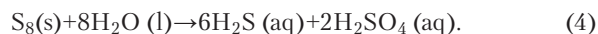
Parameter	Interpretation
$P_p \text{ CO}_2/P_p \text{ H}_2\text{S} < 20$	H ₂ S corrosion
$20 < P_p \text{ CO}_2/P_p \text{ H}_2\text{S} < 500$	Mixed corrosion
$P_p \text{ CO}_2/P_p \text{ H}_2\text{S} > 500$	CO ₂ corrosion

In this case, the ratio of partial pressure is around 10, which belongs to sour corrosion. When both CO₂ and H₂S are present, iron sulfide (FeS) film formation is faster than siderite (FeCO₃) because FeS precipitates much easier than FeCO₃. It is the reason for the absence of FeCO₃ in this case. Moreover, sulfur (S) was also found in EDS analysis, and the content was locally higher in the fracture casing. The failure area is located at the total loss area, which should not contain free sulfur segregation in the rock formation.

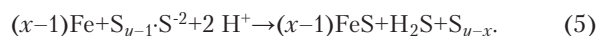
So, we can conclude that the free sulfur element is coming from the chemical reaction. The following reaction is the possible reaction to produce sulfur based on eq. (3) [15]:



Moreover, acid formation happens due to the reaction between elemental polysulfide and water at temperatures above 80 °C:



Besides hydrolysis and acidification, oxidation of iron due to polysulfide reaction makes iron sulfide



The presence of sulfur also caused a catastrophic effect on corrosion. Sulfur will form FeS crystals as shown by eq. (6) by a direct solid-state reaction for the formation of iron sulfide [15]. Reaction 4 showed the reason for the formation of FeS below the element sulfur found at tube #58–60



Moreover, at temperatures above 80 °C, oxygen could react with free sulfur to form SO₂, which oxidized further becomes SO₄²⁻ and forms a sulfuric acid in the environment.

The final result is lowering pH significantly in the corroded casing materials [16–18]. The complex reactions between oxygen, SO₂, and H₂S are shown by Sun et.al. They found that the presence of O₂, SO₂, and H₂S in the CO₂ environment could increase the corrosion rate from 0.015 mm/yr to 1.4 mm/yr [19].

From the SEM result, it appears that the Fe₃O₄ layer was formed above the FeS layer, which indicates that the presence of oxygen accelerated the corrosion as an additional reducing agent in the corrosion process. The first layer was iron sulfide. Iron sulfide has less solubility constant (KSP) than iron oxide. It made the iron sulfide as the first layer.

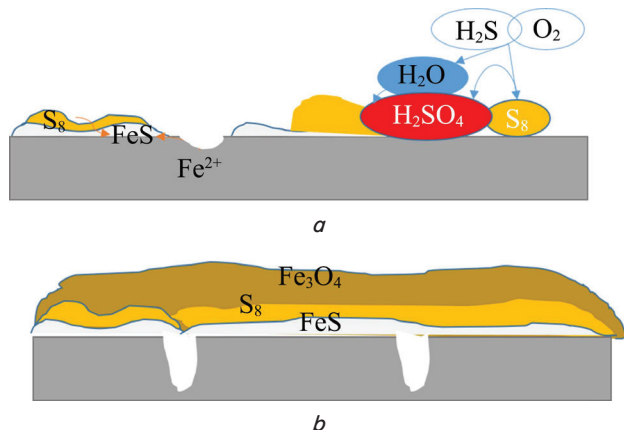


Fig. 6. Proposed mechanism of scale formation: *a* – formation of FeS as the first layer; *b* – oxidation product Fe₃O₄ is formed

In contrast, the KSP of iron oxide formation (magnetite) is higher than sulfide. The proposed corrosion mechanism is shown in Fig. 6.

The second layer was iron oxide. It was a product of further oxidation of iron hydroxide (Fe(OH)₂), which resulted

in magnetite (Fe₃O₄). Magnetite is a typical corrosion product that is formed in poor oxygen content in the environment. Air drilling process supplied and transported oxygen into the cathodic area while the anodic area will be attacked, and corrosion happened.

Some limitations of this study are the lack of data from the reservoir rock formation. This rock formation is needed to clarify the presence of a sulfur element in the reservoir.

Moreover, this study is based on real cases; hence some parameters could not be captured during the incident. In the future, laboratory and finite element simulation can be applied to support the failure analysis evidence.

However, using this failure analysis study, a lesson to learn can be achieved for future operation in an environment containing H₂S gas. So, the possibility of a similar failure incident can be reduced.

7. Conclusions

1. The failure incident happened at the total loss area, which has more possibilities of interaction with H₂S, CO₂, silica from the reservoir. The visual examination confirms that the failure incident is a corrosion-related problem.

2. Based on Norsok calculation modeling, the corrosion rate from the modeling is too low compared to the real cases, which indicated the CO₂ corrosion is not the single factor for this case.

3. The optical emission spectroscopy, tensile test, and metallography showed that the material was in good condition and met the specifications.

4. Air drilling could contribute to severe corrosion in sour service conditions. It supplied oxygen to the environment that made free sulfur ion, which could be transformed into SO₃/SO₄, which could reduce the pH of the environment.

References

1. Teodoriu, C. (2015). Why and When Does Casing Fail in Geothermal Wells: a Surprising Question? Proceedings World Geothermal Congress 2015. Melbourne. Available at: <https://pangea.stanford.edu/ERE/db/WGC/papers/WGC/2015/21041.pdf>
2. Nogara, J., Zarrouk, S. J. (2018). Corrosion in geothermal environment Part 2: Metals and alloys. Renewable and Sustainable Energy Reviews, 82, 1347–1363. doi: <https://doi.org/10.1016/j.rser.2017.06.091>
3. Seiersten, M., Nyborg, R. (2016). Modelling CO₂ Corrosion in Geothermal Systems. Proceedings of the Eurocorr. Available at: <http://eurocorr.efcwweb.org/2016/abstracts/WS%20C/67987.pdf>
4. Lyons, W. C., Stanley, J. H., Sinisterra, F. J., Weller, T. (2020). Air and Gas Drilling Manual: Applications for Oil, Gas, Geothermal Fluid Recovery Wells, Specialized Construction Boreholes, and the History and Advent of the Directional DTH. Gulf Professional Publishing, 560. doi: <https://doi.org/10.1016/c2017-0-02316-9>
5. Zhong, X., Wang, Y., Liang, J., Chen, L., Song, X. (2018). The Coupling Effect of O₂ and H₂S on the Corrosion of G20 Steel in a Simulating Environment of Flue Gas Injection in the Xinjiang Oil Field. Materials, 11 (9), 1635. doi: <https://doi.org/10.3390/ma11091635>
6. Hua, Y., Barker, R., Neville, A. (2015). Understanding the Influence of SO₂ and O₂ on the Corrosion of Carbon Steel in Water-Saturated Supercritical CO₂. CORROSION, 71 (5), 667–683. doi: <https://doi.org/10.5006/1504>
7. Hua, Y., Barker, R., Bermperidis, G., Zhao, H., Zhang, L., Neville, A. (2016). Comparison of corrosion behavior of X65, 1Cr, 5Cr and 13Cr steels in water-containing supercritical CO₂ environments with SO₂/O₂. Proceedings of Corrosion 2016. Vancouver. Available at: https://eprints.whiterose.ac.uk/101194/3/NACE_2016_FIONAL.pdf
8. Kermani, M. B., Morshed, A. (2003). Carbon Dioxide Corrosion in Oil and Gas Production – A Compendium. CORROSION, 59 (8), 659–683. doi: <https://doi.org/10.5006/1.3277596>
9. Kermani, B., Martin, J. W., Esaklul, K. A. (2006). Materials design strategy: effects of H₂S/CO₂ corrosion on materials selection. CORROSION 2006. NACE International.

10. Iannuzzi, M. (2011). Environmentally assisted cracking (EAC) in oil and gas production. *Stress Corrosion Cracking*, 570–607. doi: <https://doi.org/10.1533/9780857093769.4.570>
11. Sardisco, J. B., Pitts, R. E. (1965). Corrosion of Iron in an H₂S-CO₂-H₂O System Mechanism of Sulfide Film Formation and Kinetics of Corrosion Reaction. *CORROSION*, 21 (8), 245–253. doi: <https://doi.org/10.5006/0010-9312-21.8.245>
12. Shi, F., Zhang, L., Yang, J., Lu, M., Ding, J., Li, H. (2016). Polymorphous FeS corrosion products of pipeline steel under highly sour conditions. *Corrosion Science*, 102, 103–113. doi: <https://doi.org/10.1016/j.corsci.2015.09.024>
13. Deffo Ayagou, M. D., Joshi, G. R., Mai Tran, T. T., Tribollet, B., Sutter, E., Mendibide, C. et. al. (2020). Impact of oxygen contamination on the electrochemical impedance spectroscopy of iron corrosion in H₂S solutions. *Corrosion Science*, 164, 108302. doi: <https://doi.org/10.1016/j.corsci.2019.108302>
14. Song, Y., Palencsár, A., Svenningsen, G., Kvarekvål, J., Hemmingsen, T. (2012). Effect of O₂ and Temperature on Sour Corrosion. *CORROSION*, 68 (7), 662–671. doi: <https://doi.org/10.5006/0341>
15. Fang, H., Young, D., Nescic, S. (2008). Corrosion of mild steel in the presence of elemental sulfur. NACE - International Corrosion Conference Series. Available at: <http://www.icmt.ohio.edu/documents/publications/8172.pdf>
16. Xiang, Y., Wang, Z., Xu, C., Zhou, C., Li, Z., Ni, W. (2011). Impact of SO₂ concentration on the corrosion rate of X70 steel and iron in water-saturated supercritical CO₂ mixed with SO₂. *The Journal of Supercritical Fluids*, 58 (2), 286–294. doi: <https://doi.org/10.1016/j.supflu.2011.06.007>
17. Xiang, Y., Wang, Z., Li, Z., Ni, W. D. (2013). Effect of temperature on corrosion behaviour of X70 steel in high pressure CO₂/SO₂/O₂/H₂O environments. *Corrosion Engineering, Science and Technology*, 48 (2), 121–129. doi: <https://doi.org/10.1179/1743278212y.0000000050>
18. Hua, Y., Barker, R., Neville, A. (2015). The influence of SO₂ on the tolerable water content to avoid pipeline corrosion during the transportation of supercritical CO₂. *International Journal of Greenhouse Gas Control*, 37, 412–423. doi: <https://doi.org/10.1016/j.ijggc.2015.03.031>
19. Sun, C., Sun, J., Wang, Y., Lin, X., Li, X., Cheng, X., Liu, H. (2016). Synergistic effect of O₂, H₂S and SO₂ impurities on the corrosion behavior of X65 steel in water-saturated supercritical CO₂ system. *Corrosion Science*, 107, 193–203. doi: <https://doi.org/10.1016/j.corsci.2016.02.032>